applied optics

LARAMOTIONS: a conceptual study on laser networks for near-term collision avoidance for space debris in the low Earth orbit

Stefan Scharring,[1,*] Heiko Dreyer,[1] Gerd Wagner,[1] Jürgen Kästel,[1] Paul Wagner,[1] Ewan Schafer,[1] Wolfgang Riede,[1] Christoph Bamann,[2,6] Urs Hugentobler,[2] Pawel Lejba,[3] Tomasz Suchodolski,[3] Egon Döberl,[4] Dietmar Weinzinger,[4] Wolfgang Promper,[4] Tim Flohrer,[5] Srinivas Setty,[5,7] Igor Zayer,[5] Andrea Di Mira,[5] and Emiliano Cordelli[5]

[1]German Aerospace Center (DLR), Institute of Technical Physics, Pfaffenwaldring 38-40, 70569 Stuttgart, Germany
[2]Technical University of Munich, Institute of Astronomical and Physical Geodesy, Arcisstr. 21, 80333 Munich, Germany
[3]Centrum Badan Kosmicznych Polskiej Akademii Nauk (CBK PAN), Bartycka 18A, 00-716, Warsaw, Poland
[4]ASA Astrosysteme GmbH, Galgenau 19, 4212 Neumarkt im Mühlkreis, Austria
[5]European Space Agency – European Space Operations Center (ESA/ESOC), Robert-Bosch-Str. 5, 64293 Darmstadt, Germany
[6]Current address: Vyoma GmbH, Berliner Allee 65, 64295 Darmstadt, Germany
[7]Current address: GMV GmbH, Friedrichshafener Str. 7, 82205 Gilching, Germany
*Corresponding author: stefan.scharring@dlr.de

Received 1 June 2021; revised 14 September 2021; accepted 18 September 2021; posted 21 September 2021 (Doc. ID 432160); published 1 November 2021

A conceptual study has been carried out on laser station networks to enhance Space Situational Awareness and contribute to collision avoidance in the low Earth orbit by high-precision laser tracking of debris objects and momentum transfer via photon pressure from ground-based high-power lasers. Depending on the network size, geographical distribution of stations, orbit parameters, and remaining time to conjunction, multipass irradiation enhances the efficiency of photon momentum coupling by 1–2 orders of magnitude and has the potential to eventually yield a promisingly significant reduction of the collision rate in low Earth orbit.

https://doi.org/10.1364/AO.432160

1. INTRODUCTION

Objective of the Laser Ranging and Momentum Transfer Systems Evolution Study (LARAMOTIONS) is a conceptual analysis and feasibility study on how a (European or global) network of laser stations could significantly enhance Space Situational Awareness (SSA) and contribute to collision avoidance (CA) in the low Earth orbit (LEO). Such a ground-based laser station network, as proposed in [1], should enhance orbital data targeting for a false alert rate in conjunction warnings which, as a design parameter of this study, is 1 order of magnitude lower than the current standard.

Thus, laser tracking would yield a better view on which of the predicted conjunctions might really become critical. Avoiding them is currently restricted to CA maneuvers by active satellites involving operational costs, consumption of propellant, and therefore loss of remaining mission time. Maneuvering debris itself, however, might not only be cost-efficient but would enable avoidance of collisions where CA maneuvers are not feasible yet, namely for debris versus debris and CubeSat versus debris conjunctions.

Due to the increasing amount of space debris, several laser-based concepts for orbit modification have been proposed in the recent years. Since the sparse availability of pulsed lasers with high energy (>10 kJ) seems to render laser-ablative debris nudging for CA into a solution only for the long run [2], alternative options that can be realized earlier are mandatory to counter the rapidly increasing number of space debris in LEO. In this regard, high-power, continuously emitting (continuous-wave, cw) lasers (>10 kW) have been proposed in the past for debris nudging by photon pressure [3,4]. With momentum coupling being 3–4 orders of magnitude lower than in the case of laser ablation, this might appear as a poor alternative at first glance, but the opposite is the case when a greater number of laser stations is combined, forming an international network for laser tracking and momentum transfer (LTMT).

For laser tracking, two different use cases have been analyzed in the study: i) On-demand laser tracking (LT): on-demand

operation aims for laser fine-tracking of debris objects where collision alerts had been issued on the basis of radar data measurements. ii) Laser catalogue: a laser catalogue would constitute the outcome of an autonomous, self-standing system that continuously tracks debris objects with high precision, providing for independency from current radar data. In a certain regard, both scenarios already provide for CA since a better knowledge of orbital data reduces the associated collision probability p_c. In turn, for many events p_c would drop below the commonly accepted collision probability level (ACPL) of 10^{-4}, rendering related CA maneuvers unnecessary, since, as a result from laser tracking, the corresponding alert would turn out as a false alert; see Section 2.B.

Whereas the "laser catalogue scenario" would constitute a possible evolutionary step departing from an on-demand LT network, a different branch of such an evolution, as indicated in the study title, could be found in station networks for on-demand laser tracking including, where reasonable, momentum transfer (MT) to space debris. As a design parameter of this study, considering the potential of momentum imparted by laser photon pressure, a future LTMT system, i.e., LT and MT, should target to reduce the collision rate by 95%. Again, realistic conditions like unknown attitude and surface characteristics of the debris objects have to be reflected in the analysis; moreover, laser-based MT should not increase p_c for any other object.

The paper is organized as follows: A brief overview on the theory underlying to laser beam propagation, photon pressure, and collision avoidance will be given in Section 2, followed in Section 3 by a detailed introduction into the space debris setting of our study and the atmospheric constraints of the simulations. An outline of the main numerical methods employed in this study will be given in Section 4.

The performance of station networks for debris laser tracking is reported in Section 5 together with the background of state-of-the-art technology. Whereas findings which have been described in greater detail in a previous publication [5] are rather summarized, the focus of this overview paper is set on laser–matter interaction for momentum transfer, which is treated in Section 6. Again, the related astrodynamics analysis and LTMT network analysis of Section 7 are reported more elaborately in [5,6], respectively, and therefore are only summarized here. After summarizing our findings in Section 8, the further perspective for LTMT network implementation is sketched in Section 9.

2. THEORY

A. Beam Propagation from Ground to Debris for Deceleration by Photon Pressure

For laser beam propagation in vacuum, the second-moment beam radius w is given by [7]

$$w(z) = \sqrt{\left(\frac{M^2 \lambda\, z}{\pi\, w_0}\right)^2 + \left[w_0\left(1 - \frac{z}{f}\right)\right]^2}, \tag{1}$$

where z is the propagation distance from the transmitter, M^2 denotes the laser's beam quality parameter, λ is the laser wavelength, w_0 is the beam radius at the transmitter aperture, and f is the focal length of the beam transmitting system. As a generic laser transmitter layout choice, the initial beam radius w_0 is set to 71.5% of the aperture radius $r_T = D_T/2$, which corresponds to a 2% loss of laser power at the aperture of the telescope.

In the case of uncompensated turbulence, fluctuations of the refractive index within the beam propagation path yield significant broadening of the laser beam. In addition to that, random beam deflection, denoted as beam wander, occurs. Together with the system's mechanical beam pointing jitter σ_p, which is the standard deviation of the normally distributed residual beam pointing angle, the so-called "long-term beam radius," i.e., averaged over time, can be computed as [8]

$$w(z) = \sqrt{\left(\frac{M^2 \lambda\, z}{\pi\, w_0}\right)^2 + \left[w_0\left(1 - \frac{z}{f}\right)\right]^2 + (2\, z\, \sigma_p)^2 + 8\left(\frac{\lambda\, z}{\pi\, r_0}\right)^2}, \tag{2}$$

where r_0 is the spherical-wave coherence diameter for uplinks as given by [8]

$$r_0 = \left[0.42\, \mathrm{k}^2\, \mathrm{h}\, \sec\zeta \int_0^1 (1-\xi)^{5/3} C_n^2(\xi h)\, \mathrm{d}\xi\right]^{-3/5}, \tag{3}$$

with $k = 2\pi/\lambda$, the orbit altitude h, zenith angle ζ, and the turbulence strength $C_n^2(h)$.

If turbulence is compensated by adaptive optics, the respective system performance can be expressed by the Strehl ratio Str [9]. In addition to that, the angular uncertainty σ_t of the debris target's position as from the laser tracking can be considered as a contribution to the overall pointing uncertainty of an MT laser system, yielding

$$w(z) = \sqrt{\left(\frac{M^2 \lambda\, z}{\pi\, w_0 \sqrt{Str}}\right)^2 + \left[w_0\left(1 - \frac{z}{f}\right)\right]^2 + (2\, z\, \sigma_p)^2 + (2\, z\, \sigma_t)^2}. \tag{4}$$

For the laser radiation that is focused on the debris target, the laser-induced force from photon pressure can be computed following [10] using

$$\vec{F} = \frac{P_{\mathrm{in}}}{c_0}\left[(A + R_D)\cdot \hat{\boldsymbol{k}} - (R_D/2 + 2R_S\cos\vartheta)\cdot \hat{\boldsymbol{n}}\right], \tag{5}$$

where P_{in} is the incident laser power, c_0 denotes the speed of light in vacuum, $\hat{\boldsymbol{k}}$ is the direction of beam propagation, $\hat{\boldsymbol{n}}$ is the target surface normal, and is ϑ the beam incidence angle. The target's surface properties are given by absorptivity A, diffuse reflectivity R_D, and specular reflectivity R_S. As a generalization, Eq. (5) can be expressed using the momentum coupling coefficient $c_m = F/P$, yielding $c_m = C_R/c_0 \approx C_R \cdot 3.3\,\mathrm{nN/W}$, where $C_R \in [0; 2]$, depending on the target's properties [11]. Note that, here, $P = P_{\mathrm{in}}$ is the laser power incident at the target surface. In the case of target outshining, $P \ll P_{\mathrm{in}}$ might effectively yield $c_m \ll 3.3\,\mathrm{nN/W}$.

B. Collision Avoidance

For a debris object in LEO, the velocity decrement Δv required for its displacement Δx at the time of closest approach (TCA) depends linearly on Δx and the time span Δt between momentum transfer and TCA. Δv can be calculated from the relations for a Hohmann transfer and amounts to $\Delta x/\Delta t = 2.592\,\mathrm{km/d}$ for $\Delta v = 1\,\mathrm{cm/s}$. Considering the low momentum coupling in photon pressure, however, in reality MT would be split up in several subsequent transits during the so-called action time

frame of typically 48 h before TCA [4]. Considering the above-mentioned linearity of Δv with Δx and Δt, we assume for the sake of simplicity that the outcome of such an irradiation campaign comprising N laser engagements yielding Δv_N for each station pass would nearly equal a single irradiation 24 h before TCA with $\Delta v_1 = N \cdot \Delta v_N$. Then, 10 laser engagements with a resulting deceleration as low as $\Delta v_N = 10$ μm/s per pass would be sufficient to yield a displacement of already $\Delta x \approx 26$ m at TCA, and even more if both conjunction partners would be irradiated. In case that the debris position was known very precisely, this would be sufficient for CA. Hence, we have selected $\Delta v = 10$ μm/s as a preliminary minimum requirement for successful CA.

In reality, however, orbital data is connected with the related measurement uncertainty. Propagating this data over time, the respective uncertainty increases, which can be described by a so-called covariance ellipsoid depicting the growing uncertainty for its along-track, radial (with respect to Earth's center), and cross-track components. Therefore, these uncertainties are incorporated into collision analysis and avoidance by the numerical computation of the collision probability p_c from the overlap of the respective covariance ellipsoids at TCA—which yields a refinement of our initial MT feasibility analysis from Section 6 by including orbital dynamics in Section 7. In those simulations, for the assessment of on-demand network performance, the false alert rate (FAR) and the collision rate (CR) are employed.

We define the FAR in conjunction alerts from radar-based measurement as

$$\mathrm{FAR}^{(\mathrm{Radar})} = \frac{n_{\mathrm{FP}}^{(\mathrm{Radar})}}{n_{\mathrm{FP}}^{(\mathrm{Radar})} + n_{\mathrm{TP}}^{(\mathrm{Radar})}}, \tag{6}$$

where n_{FP} denotes the number of false positive (FP) conjunction alerts and n_{TP} gives the number of true positives (TP), respectively. For the respective assessment, the time span before the TCA is split into a decision time frame lasting up to 48 h before TCA and a subsequent action time frame in which the collision alerts are either verified, i.e., TP, or turn out to be a false alert (FP). The laser tracking system's $\mathrm{FAR}^{(\mathrm{Laser})}$ is computed with reference to the demand raised from radar measurements. Here, it has to be considered that a close approach event spotted by the radar system might be discarded by a laser tracking system, which would yield either a false negative (FN) or a true negative (TN) event in laser alerts. This is reflected by the extended definition of FAR in conjunction alerts from on-demand laser tracking in response to radar-generated alerts, given as follows:

$$\begin{aligned}\mathrm{FAR}^{(\mathrm{Laser})} &= \frac{n_{\mathrm{FP}}^{(\mathrm{Laser})} + n_{\mathrm{FN}}^{(\mathrm{Laser})}}{n_{\mathrm{FP}}^{(\mathrm{Radar})} + n_{\mathrm{TP}}^{(\mathrm{Radar})}} \\ &= \frac{n_{\mathrm{FP}}^{(\mathrm{Laser})} + n_{\mathrm{FN}}^{(\mathrm{Laser})}}{n_{\mathrm{FP}}^{(\mathrm{Laser})} + n_{\mathrm{TP}}^{(\mathrm{Laser})} + n_{\mathrm{FN}}^{(\mathrm{Laser})} + n_{\mathrm{TN}}^{(\mathrm{Laser})}}.\end{aligned} \tag{7}$$

Concerning CR, we use the following definition for an all-on-all conjunction analysis where CR is defined by $\mathrm{CR} = \sum_j p_{c,j}$ as the sum over all collision probabilities of possible conjunction pairs j. CR can thus be reduced by i), enhancing the quality of orbital data by precise, e.g., laser, measurements, which reduces the related covariance and/or ii) by modification of the trajectories themselves by a CA maneuver.

3. ENVIRONMENTAL CONTEXT OF LTMT NETWORKS

A. Space Debris Environment

The study focuses on a dedicated subset—denoted as the operational orbital regime (OOR) of the LEO space environment, by a mean altitude of $h \in [579; 1179]$ km, an orbit inclination of $i \in [65°; 110°]$, and a numerical eccentricity of $\varepsilon \in [0.0; 0.2]$. For our work, we have selected a snapshot of orbital data from the catalogue of the United States Strategic Command (USSTRATCOM) as of 2 July 2019, which has been filtered correspondingly with respect to h, i, and ε, yielding overall 10,916 objects comprising:

- 1077 active satellites, which must not be irradiated,
- 1467 integer debris objects like defunct payloads, orbiting rocket bodies, or out-of-use mission-related objects for which information about mass m, shape, and optical cross section A_{cs} can be assigned using an extract of ESA's Database and Information System Characterizing Objects in Space (DISCOS) [12],
- 611 further integer objects for which either no information on m or A_{cs} is available, and
- 7634 fragments from explosions and collisions, where neither information on m or shape can be retrieved from DISCOS, but only the radar cross-sectional area A_{rcs}. For them, m and A_{cs} have been estimated using ESA's Meteoroid and Space Debris Terrestrial Environment Reference (MASTER) [13].

Discarding integer debris objects with incomplete data as well as active satellites, this results in 9101 different debris objects which are considered in our study. Their two-line element (TLE) orbital data is employed in the laser tracking network studies reported in Sections 5.F and 5.G, whereas information on mass, shape, optical cross section and, where applicable, average orbital altitude is used for the simulations on laser–matter interaction shown in Section 6. Using the results of the latter simulations, the LTMT network simulations of Section 7.B incorporate both target properties and their orbital data. In contrast to those simulations addressing the entire OOR, the more fundamental astrodynamics simulations discussed in Sections 5.E and 7.A have been restrained to representative OOR target samples.

B. Weather Constraints

Ground-based laser operations in orbit are frequently constrained by cloud cover where beam transmission is entirely blocked (except for thin cirrus clouds [14]). This is reflected in the network analyses of Sections 5 and 7 (see below), by a randomized distribution of outage intervals, denoted as duty cycle. As an empirical outcome from laser tracking observations, a total cloud cover of CF = 50% can be deemed an (optimistic) upper feasibility limit for outdoor laser operations to space [15]. Hence, we have used weather data on cloud cover [16] to derive site-specific laser access rates, i.e., the time fraction where $\mathrm{CF} \leq 50\%$.

Moreover, the laser beam can significantly be attenuated by scattering and absorption from aerosols and air molecules, which in particular reduces the performance of laser-based MT. In the network simulations, we have employed global weather

data of the aerosol optical depth (AOD [17,18]) to derive average values for the site-specific beam transmission that can be computed using $T(\lambda, \zeta) = I/I_0 = \exp[-\mathrm{AOD}(\lambda) \cdot \sec\zeta]$. Whereas this data has been used in the LTMT network analyses depicted in Section 7.B, the MT feasibility study shown in Sections 6.D–6.F has been undertaken using the atmospheric attenuation model at $\lambda = 1.06\,\mu\mathrm{m}$ for "clear" conditions, i.e., 23 km visibility range, from [19], which corresponds to AOD = 0.144. Further details on AOD and CF weather data usage in this study can be found in [5].

Finally, we have used the Hufnagel–Andrews–Philipps (HAP) model for daylight conditions for the simulations of atmospheric turbulence, which exhibits a better modeling for the ground layers than, e.g., Hufnagel–Valley 5/7, and is, concerning the LTMT network simulations, less idealistic than astronomical models like, e.g., Cerro Pachón [20].

4. NUMERICAL METHODS

A. Laser–Matter Interaction

To consider the dependencies of laser-exerted force from incidence angle and surface properties for different target geometries, the DLR code Examination Program for Irregularly Shaped Debris Targets (Expedit) is used, which combines discretization of laser beam and target surface for parallelized momentum computation. The code had formerly been developed for calculation of laser-imparted momentum in laser ablation and is described in greater detail in [21]. An interaction module for photon pressure had been developed subsequently and is firstly employed in this study.

For the simulation targets, simple geometries have been derived using shape information from DISCOS data (cf. Section 3.A) and applying some simplifications for complex geometries like, e.g., a "cylinder + cone" rocket body or a "box + panels + antenna" payload, which we have modeled by generic cylinders, cuboids, or ellipsoids, respectively, exhibiting a similar optical cross section. Finally, the debris fragment population has been generated by a statistical approach using an estimate of A_{cs} from DISCOS data on A_{rcs} and generating a statistical distribution of axis ratios X/Y and Y/Z in agreement with the fragment statistics from ground-based satellite crash tests [22]; cf. [21] for more details on this method. An overview on shapes and axis ratios for all 9101 OOR targets is given in Fig. 1. The target geometry for each debris object has been represented by a corresponding geometry definition file in OBJ format (Wavefront Technologies).

Following [23], we have assumed an albedo $R_A = 1 - A = 0.275$ for fragmentation debris and $R_A = 0.12$ for integer targets, respectively, for the simulations of laser–matter interaction. For the sake of simplicity, we have set $R_D = R_S = 0.5 \cdot R_A$.

B. Ground-Based Laser Tracking and Momentum Transfer

For the analysis of laser tracking networks, the Python simulation environment from a previous study on laser networks [15] has been extended and parallelized. It serves as the backbone for execution of the software products Systems Tool Kit and Orbit Determination Tool Kit from Analytical Graphics, Inc. as well as for related data pre- and postprocessing. The simulation environment comprises six tools:

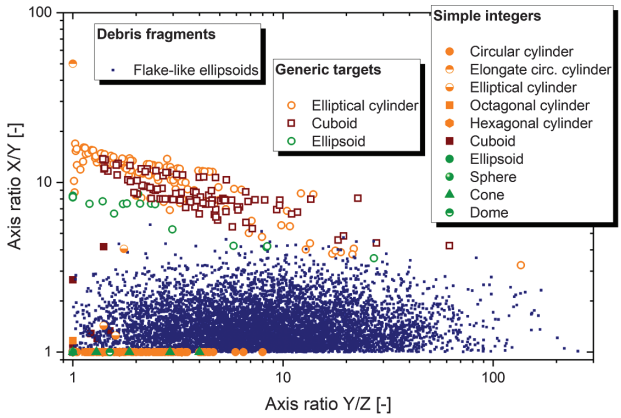

Fig. 1. Axis ratios of OOR simulation targets.

First, the Reference Trajectory Generator applies a least-squares fit on TLE data in order to generate reference trajectories for each object. Second, FAR and CR of a radar tracking system are derived from analyses with a Radar Tracking Simulator. Furthermore, close approach warnings are created here, and reference trajectories are generated from real-world conjunction data messages (CDM). Subsequently, the Compute Passes Tool generates tracklets and measurement samples for a given network geometry, which is created by the Network Generator from a station database. The Laser Tracking Simulator finally simulates the actual laser tracking process, yielding FAR and CR of the laser system, which can then be compared with the respective values of the radar system. Moreover, a list of station-specific random outage time intervals is created in the Duty Cycle Generator (cf. Section 3.B) and applied on the tracklets.

For the simulation of LTMT networks, a Momentum Transfer Simulator has been added, which generates the trajectories modified by laser MT. Here, randomized MT thrust vectors are generated for the computed passes by interpolating tabulated laser–matter interaction data from simulations with the Expedit code; cf. Section 6.F. These thrust vectors are applied to the debris trajectories, yielding new laser tracking measurement values for the modified trajectories and, correspondingly, the resulting CR after orbit modification. Furthermore, an algorithm for the determination of an optimum illumination strategy, i.e., whether to accelerate or decelerate the target, has been developed.

Further details on the code and the respective simulations are given in [5].

5. LASER TRACKING

A. Passive-Optical Target (Re-)acquisition

Generally speaking, imaging-based object tracking is only possible if the object is illuminated by the Sun in front of a dark sky background so that the camera can record the object without being saturated. Then, laser ranging is even possible without any wavelength filtering or temporal gating; however, blind tracking performance and orbit prediction need to be good enough, depending on tracking laser beam divergence and the detector's field of view, to ensure that the signal is collected by the single photon detector. For daylight tracking, imaging methods are

more difficult to apply due to the high amount of background radiation from the Sun and sunlight scattered in the atmosphere. Therefore, usage of imaging methods for daylight tracking is not considered within this activity. On the other hand, the lack of sunlight illumination impedes passive-optical target acquisition for those times during nighttime when the object is in Earth's shadow, which in turn depends on its orbital parameters, the period of the year, and the station's position.

Orbit propagation uncertainties significantly drop after a laser ranging measurement enabling accurate orbit prediction, e.g., using near-real-time data filtering and orbit determination by an extended Kalman filter (EKF) [24]. Then, during a certain time span after laser ranging (cf. Section 5.D), this prediction can serve as a basis for blind tracking, i.e., without the need for passive-optical target reacquisition and, therefore, suitable for 24/7 operation regardless of the Sun's illumination.

B. Technological Options for Tracking Lasers

For laser tracking of space debris, pulsed high-power lasers are used [25–28], e.g., diode-pumped, Q-switched Nd:YAG lasers emitting at $\lambda = 1064$ nm or at the second harmonic ($\lambda = 532$ nm) with pulse lengths τ in the nanosecond range and pulse energies in the range of $E_L = 25$ mJ up to $2\,J$. Concerning λ, a trade-off has to be undertaken considering available laser power, beam divergence, atmospheric attenuation, laser safety, and public awareness.

The tracking accuracy directly depends on the control process and the accuracy of the drive system and intermediate mechanics. Sources of systematic errors can arise from ephemeris data, calculations, telescope reference frame mapping, optical directional mismatch, time scale errors, and laser beam wander due to atmospheric turbulence. Angular errors in laser beam pointing can result from vibrations and mechanical misalignment. Systematic telescope observation errors are typically modeled using a pointing model based on observed fixed star positions; however, this is limited by atmospheric flickering.

Under twilight conditions, any remaining error while tracking an object can be corrected by measuring the apparent angle of the object using a camera while having the telescope mount position in a closed loop. Typically, the apparent angle can be measured within 1 arcsec accuracy without adaptive optics and 0.1 arcsec with state-of-the-art adaptive optics. If the pointing model and orbit prediction are better than the field of view of both the detector for laser ranging and of laser beam pointing of the transmitted laser, then 24/7 tracking regardless of Sun illumination is possible, keeping the target in a closed loop, maximizing the number of photons returns from laser ranging.

C. Astrodynamic Constraints of Laser Tracking

The performance of a network of ground stations for laser tracking is ruled by several site-related constraints: In the long-term average over the OOR, the target revisit frequency for a particular station strongly increases with the geographical latitude of the station—from 2.5/day for equatorial laser sites up to 10 for polar sites. Moreover, the ability for passive-optical target (re-)acquisition largely depends both on geographical latitude and time of the year: averaged over all OOR debris targets, the terminator duration increases from approximately 1 h (equatorial) up to 3 h (polar) in the annual mean, while strong seasonal deviations from this average exist, especially for the stations beyond the polar circle with no twilight times during the polar night and up to 8 h in midsummer.

D. Orbit Propagation

The along-track orbit uncertainty σ_I is highly driven by drag force errors, especially in lower orbital altitudes—primarily as a result from errors σ_ϱ in the thermospheric density model and particularly pronounced for objects with a large ballistic coefficient BC. As an example, orbital data from an object with $\mathrm{BC} = 0.01\ \mathrm{m^2/kg}$ would exhibit an orbit prediction uncertainty of only $\sigma_I = 10 \ldots 50$ m after 3 days of propagation for a circular orbit at $h = 700$ km altitude, whereas at in the more dense residual atmosphere at $h = 550$ km the uncertainty would be in the range of $\sigma_I = 50 \ldots 230$ m. Hence, the drag-related uncertainty can be controlled well through frequent laser tracking in the higher-altitude orbit, while in the lower-altitude orbit it may already exceed the uncertainty limit for blind tracking after several hours.

This limitation, denoted in the following as laser tracking data expiry time τ_{LT}, can be computed from the beam divergence of the tracking laser using a beam-target hit probability model as lined out in greater detail in [5]. Using an initial elevation of $\varepsilon_{\mathrm{blind}} = 15°$ with an initial tracking laser beam divergence of 30 arcsecs, the maximum permissible along-track uncertainty for 24/7 tracking $\sigma_{I,\max}$ amounts to 210 m ($h = 580$ km) up to 330 m ($h = 1180$ km), respectively. In turn, this corresponds with the time span τ_{LT} after the last laser ranging measurement during which the covariance of orbital data increases again. Analysis of the temporal evolution of covariance for OOR objects gives an empirical fit function with

$$\tau_{LT} \approx 54\ \mathrm{min} - 0.05\ \mathrm{min/km} \cdot h + 0.00113\ \mathrm{min/km^2} \cdot h^2,$$

i.e., the time between two laser ranging measurements must not exceed approximately 7 h for low OOR orbits but can amount up to ca. 26 h for high altitudes in the OOR.

Especially when tracking objects already at low elevations, the along-track orbit uncertainty can then be significantly reduced, even with the first observation. With a near-real-time EKF framework, it is possible to almost immediately reach an orbit accuracy that is sufficiently accurate to start closed-loop tracking for laser momentum transfer, even if the orbit uncertainty grows above 50 meters and more during observation gaps.

E. Laser Tracking Feasibility Study

In an initial feasibility study on laser tracking networks, a small European network with stations in Borowiec (Poland), Wettzell (Germany), and Graz (Austria) as well as a small global network with stations in Borowiec, Mt. Stromlo (Australia), Haleakala (Hawaii, USA), Greenbelt (Maryland, USA) have been analyzed using a ballistic coefficient of $\mathrm{BC} = 1\ \mathrm{m^2/kg}$, a laser ranging precision of $\sigma_r = 1.5$ m (discarding bias), and high-fidelity force models assuming 15% uncertainty of thermospheric density but discarding errors from solar radiation pressure. In addition, it is assumed that blind tracking is possible; moreover, different duty cycles have been analyzed, reflecting constraints arising, e.g., from weather conditions or observation scheduling. The results (cf. Fig. 2 for a typical example) confirm the feasibility of using laser tracking to produce very accurate orbits, which can be used to commence laser MT—provided that model-based errors introducing biases can be controlled well enough.

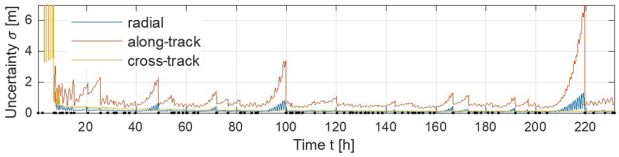

Fig. 2. Sample of temporal evolution of orbital data covariance in a global laser tracking network with four stations at a tracking success rate of 50% (considering outages, e.g., due to cloud cover). The observed debris target is on a circular orbit at 750 km altitude with 52° inclination. Laser ranging measurements are indicated by the black dots on the x axis and comprise 1 normal point per 10 s.

F. Use Case #1: Networks for Laser Tracking in Response to Collision Alerts

In a more elaborate study using the simulation environment lined out in Section 4.B, three different networks have been investigated for the use cases on-demand laser tracking and laser catalogue: As a starting point a small European network (SEN) comprising five stations (Tenerife, Spain; Herstmonceux, Great Britain; Borowiec, Poland; Metsähovi, Finland; Murfatlar, Romania) has been configured. For network extension, two different strategies have been addressed: i) increasing the number of stations only regionally and ii) increasing the number of stations and simultaneously the network extension. For the latter, four stations (Haleakala, Hawaii, U.S.; San Juan, Argentina; Hartebeesthoek, South Africa; Mt. Stromlo, Australia) have been added, yielding global coverage in a large extended network (LXN) (cf. Fig. 3), whereas for the former, three other European stations (Grasse, France; Graz, Austria; Tromsø, Norway) have been added to the SEN now constituting a large European network (LEN, not shown in Fig. 3). As a summary it can be stated that for on-demand laser tracking, the LXN is sufficient to bring both the FAR and the CR below the values of the system requirements; cf. Table 1.

G. Use Case #2: Networks for an Autonomous Space Debris Laser Tracking Catalogue

For the use case of autonomous laser tracking of all OOR objects, a global network coverage is desirable, since it improves the results by a factor of 2–3, as can be seen from the comparison between the LEN and LXN data shown in Table 2. However, it

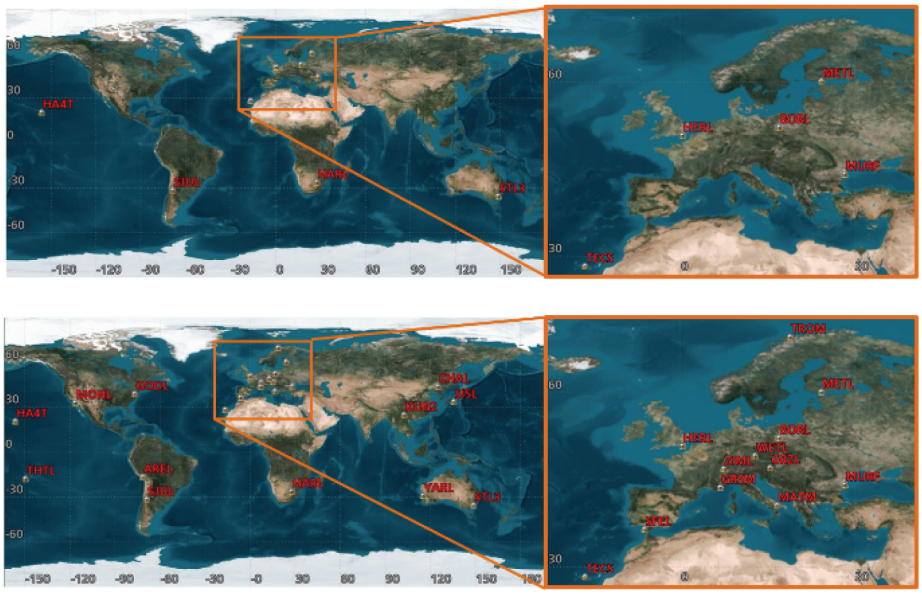

Fig. 3. Upper graph: Map of the large extended (LXN) network. The small European network (SEN), which is part of LXN, is shown in the right image. Lower graph: Map of the extra-large extended (XXN) laser station network (analyzed only in use cases #2 and #3). Figures taken from [5], used with permission.

Table 1. Dependency of Collision Rate and False Alert Rate from Laser Tracking Network Configuration and Duty Cycle[a]

		Collision Rate			False Alert Rate		
Week	Duty Cycle	SEN	LEN	LXN	SEN	LEN	LXN
A	50%	$2.7 \cdot 10^{-3}$	$3.3 \cdot 10^{-3}$	$1.8 \cdot 10^{-22}$	0.057	0.060	0.065
A	Site-specific	$1.0 \cdot 10^{-3}$	$1.4 \cdot 10^{-3}$	$1.1 \cdot 10^{-24}$	0.064	0.062	0.058
B	35%	$2.7 \cdot 10^{-5}$	$2.2 \cdot 10^{-6}$	$1.1 \cdot 10^{-13}$	0.028	0.028	0.007
B	50%	$1.4 \cdot 10^{-6}$	$1.8 \cdot 10^{-8}$	$6.2 \cdot 10^{-15}$	0.034	0.021	0.014
B	Site-specific	$5.3 \cdot 10^{-5}$	$2.9 \cdot 10^{-6}$	$2.9 \cdot 10^{-7}$	0.007	0.007	0.021

[a]Reference values for performance of the radar system: CR = $2.24 \cdot 10^{-2}$ (week A), and $6.46 \cdot 10^{-3}$ (week B), resp., FAR = 0.78 (both weeks). Simulation weeks are (A) 12–18 July and (B) 1–7 September of 2019.

Table 2. Dependency of Laser Catalogue Capacity from Tracking Network Configuration and Duty Cycle[a]

	European Networks		Global Networks	
Duty Cycle	SEN	LEN	LXN	XXN
35%	436 ± 29	648 ± 19	1035 ± 74	n.d.
50%	660 ± 43	871 ± 35	1482 ± 24	n.d.
Site-specific	624 ± 44	825 ± 40	1787 ± 79	n.d.
100%	1226	1366	3032	5448

[a]For the XXN, the impact of duty cycle on network capacity has not been analyzed.

has been found that with the LXN, even a global network of nine stations is insufficient for continuous catalogue maintenance. Instead, the catalogue capacity, i.e., the number of objects that can be tracked without the need for target reacquisition, amounts to less than 2000 for the LXN under realistic weather conditions. Nevertheless, in order to fulfill both requirements, a network with substantially more than nine stations would be required, presumably more than 100 in the case of a 50% duty cycle, which has not been analyzed within the study due to time constraints.

6. LASER–MATTER INTERACTION FOR MOMENTUM TRANSFER TO SPACE DEBRIS

A. Technological Options in High-Power Lasers and Transmitters

The large distances from ground to debris in LEO make great demands on the focusability of the laser beam, which rule out both the usage of multimode lasers or employing laser radiation at great wavelengths like, e.g., $\lambda = 10.6\ \mu$m as for CO_2 lasers [cf. Eq. (1)]. Concerning the near-term assumptions on high-power laser technology, as seen from today, solid-state lasers are the most promising candidates for usage in such a network. Beam coupling of cw high-power lasers would likely end up with a laser power of 40 kW for momentum transfer. For MT laser operation, the near-infrared range is clearly recommended, represented here by ytterbium-doped lasers at $\lambda = 1070$ nm. Like for laser tracking, a superior beam quality of $M^2 \leq 1.5$ is required to meet the requirements of the final network. Since momentum transfer requires a precise knowledge of the object's position, a hybrid station concept is proposed where in the optimum case MT and LT laser systems are coupled within a single Coudé beam path of, e.g., a Ritchey–Chrétien telescope.

B. Monte Carlo Analysis of Geometric Constraints in Laser–Debris Interaction

From Eq. (5) several uncertainties in the expected magnitude of laser-imparted force by photon pressure to space debris can be derived: Insufficient knowledge about the surface properties as well uncertainties about the incidence angle of the laser beam limit the predictability of imparted momentum and its direction. The major impact on laser-induced force, however, comes with the debris' size and orientation, since this affects the optical cross section and therefore the losses from target outshining. Hence, similar to our previous work shown in [21], we have carried out Monte Carlo studies for each one of the 9101 OOR objects in which laser–matter interaction has been simulated for different randomly chosen target orientations using a uniform distribution for the Eulerian orientation angles. With the deliberate computational constraint of using $N_S = 11$ samples at least, but not exceeding $N_S = 1000$, Monte Carlo sampling has been monitored in each simulation, using as a stop criterion for $11 < N_S < 1000$ that the accuracy $\sigma_{CI} = 1.96 \cdot \sigma_X/\sqrt{N_S}$ of the 95% confidence interval of the imparted force alongside the beam axis has to be less than 10% of the average value X of the coaxial force component (and likewise for the fraction of laser energy, which reaches the target's surface).

As an outcome of this study it has been found that the dependency of the radiation pressure coefficient C_R from the area ratio of optical cross section to laser spot size can be approximated by the following empirical expression:

$$C_R\,(A_{cs}/A_s) \approx a_1 \left[1 - \exp\left(-\frac{A_{cs}/A_s}{b_1}\right)\right] + a_2 \left[1 - \exp\left(-\frac{A_{cs}/A_s}{b_2}\right)\right], \quad (8)$$

where a_1, a_2, b_1, and b_2 are fitting parameters that depend on target geometry type (cf. the geometry categories listed in the legend of Fig. 1), surface properties (absorption, diffuse reflection, specular reflection or the albedo settings described in Section 4.A), and, in particular, the members of the respective debris target subset itself. As an example, the dependency of C_R from the area ratio is shown for spherical targets in Fig. 4.

C. Atmospheric Constraints of Laser Momentum Transfer from Ground to Space Debris

As a preliminary feasibility assessment of MT for collision avoidance the idealized scenario of a direct transit of a debris object through the zenith of an LTMT station has been assessed. In the simulations, the target is irradiated on its ascending path in order to lower its in-track velocity as outlined in greater detail in [29]. The impact of MT irradiation on radial Δv and the corresponding trajectory modification is significantly lower and therefore discarded in this simulation. Moreover, cross-track Δv does not occur, since a direct station transit has been chosen for the sake of simplicity. In contrast, all Δv components are considered in the LTMT network simulations lined out below in Section 7.B.

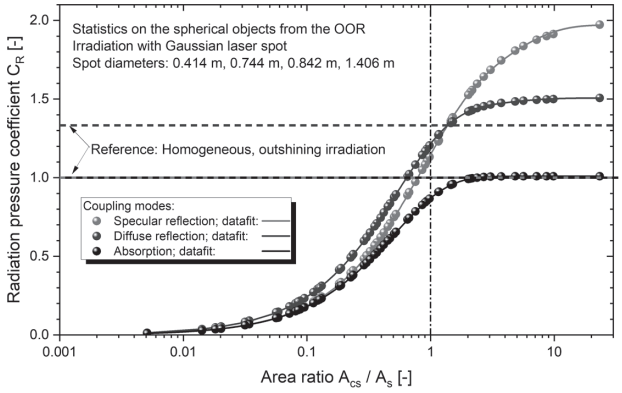

Fig. 4. Radiation pressure coefficient for a spherical target as function of irradiation size ratio.

For the simulations we have chosen $P_L = 40\,\text{kW}$, $\lambda = 1070\,\text{nm}$, $M^2 = 1.5\,\text{m}$, $D_T = 2.5\,\text{m}$ for the MT ground station, which irradiates the target for $\zeta \in [10°; 80°]$ on its ascending path. Atmospheric attenuation is modeled using $\text{AOD} = 0.144$, and we imply the transmitter's agility to dynamically adjust its focal length to the actual distance z to the target, i.e., $f(t) \equiv z(t)$ throughout the entire irradiation [cf. Eq. (1)], which is computed from ζ and the object's particular average orbital altitude h. As a worst-case scenario, atmospheric turbulence has been assumed using Eq. (2) for the computation of the beam spot size at the debris position. Anticipating that atmospheric beam wander would have a much larger impact than mechanical pointing errors, we have set $\sigma_p = 0$. Note that Eq. (2) gives a long-term average beam radius, whose usage here is justified by the linearity of photon pressure with respect to incident laser power [cf. Eq. (5)]. For laser ablation, in contrast, the strong nonlinearity of momentum coupling with incident fluence (cf., e.g., [30]), would not permit such an assumption.

For comparison, atmospheric turbulence has been discarded using Eq. (1) as a best-case baseline scenario. As can be seen from Fig. 5, uncompensated atmospheric turbulence restrains the imparted laser force by 1 up to 2 orders of magnitude, which in particular affects smaller targets due to large outshining losses. Hence, turbulence compensation is mandatory to reduce beam broadening and beam wander. On the other hand, it can be derived from the results that the requirements for turbulence compensation are likely to be more relaxed for the great multitude of small fragments than for the more massive integer objects.

D. Analysis of Turbulence Compensation for Laser Power Beaming

In laser tracking the light reflected from the space debris arrives at the ground station from a particularly different angle than where the debris particle actually is and, likewise, the high-power laser beam has to be emitted into yet another direction to be able to hit the space debris. The corresponding point-ahead angle is in the range of several tens of microradians, and

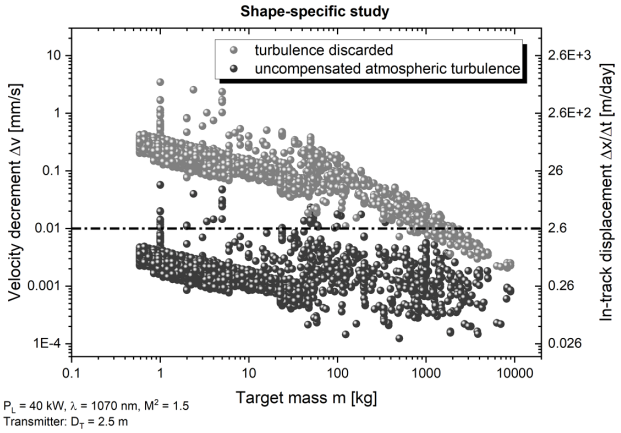

Fig. 5. Impact of atmospheric turbulence on the velocity decrement Δv for all 9101 OOR targets under irradiation during a direct station transit for $\zeta \in [10°; 80°]$ by a high-power laser beam ($P_L = 40\,\text{kW}$, $M^2 = 1.5$), transmitted by a telescope of 2.5 m aperture diameter. The estimated minimum requirement for collision avoidance of $\Delta v = 10\,\mu\text{m/s}$ is indicated by the dash-dotted line.

therefore smaller than the isoplanatic angle for tip/tilt contributions. It is hence possible to measure tip/tilt from the debris signal. Since such tip/tilt information cannot be determined otherwise, e.g., from a laser guide star (LGS), we assume in the following that tip/tilt is indeed found from the light reflected from the debris target. Contrary to the tilt information, the point-ahead angle between high-power laser and debris signal is larger than the corresponding isoplanatic angle for higher-order aberrations. If left uncorrected, such spatial high-frequency aberrations would lead to significant decorrelation between the two directions and render successful correction of higher-order aberrations impossible. Hence, a laser guide star has to be used as a means of acquiring valid information about higher-order aberrations. Angular decorrelation between the direction where the LGS signal arrived from and the direction into which the high-power laser has to be emitted can be eliminated by assuming that the LGS points ahead of the high-power laser by some additional microradians. By choosing the point-ahead angle between LGS and high-power laser correctly, we can make sure that the wavefront information acquired from the LGS signal has arrived just from the direction where the laser will have to aim after the time needed for the light to travel from the LGS, the wavefront to be measured, and the signal processed. This amount of time will in the following be referred to as LGS response time.

The information about the atmospheric distortions will therefore and unavoidably have aged during the LGS response time before actually being imprinted onto the wavefront of the laser as it leaves the telescope. Such temporal decorrelation between the laser wavefront and the momentary status of the atmospheric eddies are covered by the Greenwood frequency f_G and yield a contribution $S_{\text{temp}} = \exp[-(f_G/f_{3\,\text{dB}})^{5/3}]$ to the overall Strehl ratio Str of the system. The frequency $f_{3\,\text{dB}}$ corresponds to the characteristic frequency of the actuator response function. Note that for deformable mirrors, $f_{3\,\text{dB}}$ will typically not exceed a few hundred hertz. Assuming camera readout and computational processing to happen within less than 1 ms, the LGS response time is typically significantly shorter than the actuator response time. The overall system response function will therefore be primarily governed by the response function of the deformable mirror.

A second major contribution to Str results from the residual mismatch between the actual deformed surface of a deformable mirror and the aberrated wavefront, which depends on the spatial density of actuators on the transmitter and can be described using $S_{\text{zonal}} = \exp[-0.32(r_s/r_0)^{5/3}]$, where r_s is the distance between the actuators. It can be shown that a telescope with $D_T = 2.5\,\text{m}$ is easier to correct than for $D_T = 4.0\,\text{m}$. Moreover, after the initial steep increase of S_{zonal} with the number of actuators, the performance of the compensation system can only be slightly enhanced by further addition of actuators.

The third contribution to Str comes from the so-called cone effect that can be quantified using $S_{\text{cone}} = \exp[-(D_T/d_0)^{5/3}]$, where d_0 is defined for the altitude h_{LGS} of the LGS spot in a way similar to r_0 [cf. Eq. (3)] by $d_0 = [0.501\,k^2 h_{\text{LGS}} \sec\zeta \int_0^1 \xi^{5/3} C_n^2(\xi h)\text{d}\xi]^{-3/5}$ [31]. The cone effect denotes the error of the measured wavefront due to i) the residual fraction of atmospheric volume through which the MT laser propagates but which is not sampled by the LGS

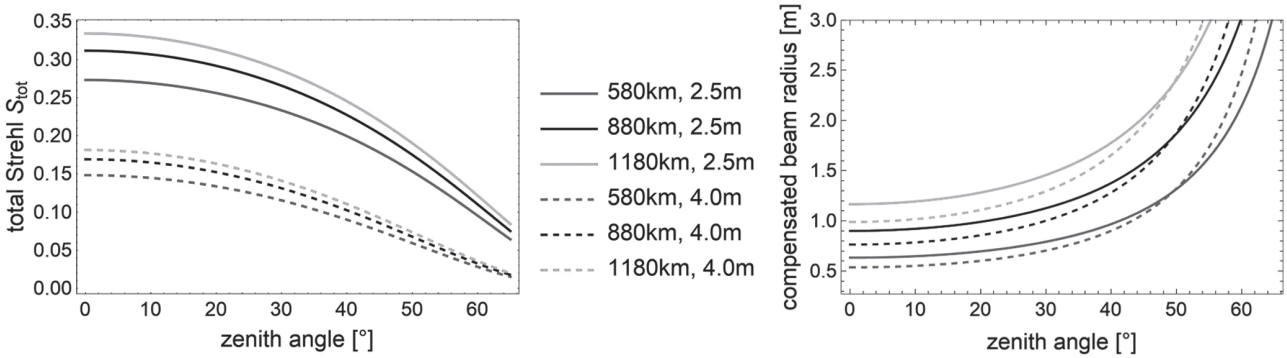

Fig. 6. Overall Strehl ratio and resulting (short-term) radius of the laser beam focused on a debris object at various orbit altitudes for two different transmitter apertures as a function of the beam pointing zenith angle.

and ii) the disproportional weighting of the information about elevated atmospheric layers contained in the LGS wavefront.

Finally, the overall $Str = Str(h, \zeta) = S_{\text{temp}} \cdot S_{\text{zonal}} \cdot S_{\text{cone}}$ can be seen from Fig. 6. The number of actuators was set to 300, and the bandwidth $f_{3\,\text{dB}}$ of the deformable mirror to 300 Hz. These certainly are demanding specifications for a large high-power deformable mirror but should be reachable within the next few years.

In addition to the turbulence compensation of beam broadening, a piezo-driven tip/tilt correction has to be applied in MT laser pointing yielding a residual pointing uncertainty of approximately 0.01 arcsecs.

E. Impact of Adaptive Optics Usage and Tracking Precision on Imparted Momentum

With these specifications of the adaptive optics system, the feasibility study shown in Section 6.C has been repeated employing $Str(h, \zeta)$ and the residual pointing uncertainty in Eq. (4). Note that in the following, the irradiation interval has been constrained to $\zeta \in [15°; 65°]$, since too small zenith angles yield only poor in-track deceleration, whereas too small elevation angles would require an unrealistically large no-flight zone or very high efforts in airspace surveillance.

As a metrics for this study, a momentum transfer efficiency $\eta_{MT} = \Delta v/\Delta v_0$ is introduced, relating the velocity decrement Δv in a simulation to the Δv_0 that would be obtained for the respective target if the laser light would simply propagate through vacuum, i.e., discarding all atmospheric effects. Using this definition, it can be seen from Table 3 that atmospheric extinction lowers the efficiency of momentum transfer by 20%. Moreover, in the case of uncompensated turbulence, only a poor momentum transfer efficiency of 2.5% remains. If, however, as outlined in the previous subsection, adaptive optics is used for turbulence compensation together with tip/tilt compensation for beam pointing jitter, the overall momentum transfer efficiency amounts to 20% on average, which is 1 order of magnitude better than in the case of uncompensated turbulence.

Using the latter (compensated) case as a new baseline, the uncertainty from laser tracking can now be included as an additional constraint for the overall performance of MT. As a corresponding metrics, the tracking-related momentum transfer efficiency $\eta_{\text{LT}} = \Delta v/\Delta v_{ao}$ is introduced, relating the simulation results to the findings of Δv_{ao} for the respective targets assuming $\sigma_t = 0$. From the related simulations, summarized in Table 4, it can be concluded that the laser tracking uncertainty has a significant impact on the long-term laser spot size as of Eq. (4): already a tracking uncertainty of 0.1 arcsecs reduces the efficiency of momentum transfer down to 70%. With $\sigma_t = 0.2''$, momentum transfer efficiency goes down to 35% and further to 20% at $\sigma_t = 0.3''$. Mapping this with the preliminary assessment for the minimum requirement for collision avoidance, $\Delta v = 10$ μm/s, one can conclude that CA is still feasible for the majority of the objects at $\sigma_t = 0.1''$, whereas this ability almost vanishes at $\sigma_t = 0.3''$.

As an outcome of this feasibility assessment, it can be concluded that successful collision avoidance can be undertaken for the majority of the OOR objects using a transmitter of 2.5 m diameter, equipped with 300 actuators for the adaptive optics, operating with a bandwidth of 300 Hz, provided a laser tracking precision of only 0.1 arcsecs can be achieved. This accuracy appears to be technically feasible but demands for laser guide star (LGS) usage not only in uplink for turbulence-compensated beam transmission of the MT laser and ranging laser but as well at the optical downlink path, with a second LGS, for turbulence compensation of the tracking signal from the debris object.

Table 3. Momentum Transfer Efficiency η_{MT} [%] under Atmospheric Constraints of Attenuation and Turbulence[a]

Turbulence	Simple Integers	Generic Targets	Fragments	All Targets
Discarded	79.4 ± 0.5	79.7 ± 0.3	80.53 ± 0.04	80.4 ± 0.4
Uncompensated	13.0 ± 11.5	5.5 ± 3.7	1.04 ± 0.06	2.5 ± 5.2
Adaptive Optics	51.7 ± 22.0	33.0 ± 8.4	15.4 ± 0.9	20.1 ± 13.4

[a]In the reference case, both extinction and turbulence are neglected. Performance losses from tracking uncertainty are discarded in the simulations, i.e., $\sigma_t = 0$.

Table 4. Tracking-Related Momentum Transfer Efficiency η_{LT} [%] for Turbulence Compensation Using Adaptive Optics and Tip/Tilt Compensation of Beam Pointing Jitter as Specified in Section 6.D[a]

σ_t [arcsec]	Simple Integers	Generic Targets	Fragments	All Targets
0.1	83.9 ± 11.8	77.8 ± 6.7	63.9 ± 1.2	66.7 ± 7.8
0.2	59.8 ± 20.0	49.9 ± 10.5	31.4 ± 1.1	35.3 ± 11.5
0.3	41.8 ± 19.9	32.5 ± 10.0	17.1 ± 0.7	20.5 ± 10.4
0.5	21.8 ± 14.4	15.9 ± 7.0	7.0 ± 0.3	9.0 ± 6.8
1.0	6.9 ± 5.8	4.9 ± 2.9	1.9 ± 0.1	2.5 ± 2.5

[a]In the reference case, performance losses from tracking uncertainty are discarded, i.e., $\sigma_t = 0$.

F. Target-Specific Laser–Matter Interaction

Finally, two simplifications that were used in Sections 6.C and 6.E were replaced by explicit numerical simulations in order to achieve more accuracy in momentum prediction.

First, instead of the shape-specific fitting functions for C_R, cf. Eq. (8), target-specific results have been computed using Expedit for each debris object. For this purpose, laser-induced momentum is derived for each one of the 9101 OOR targets under different zenith angles $\zeta = 15°, 20°, 25°, \ldots, 65°$ considering turbulence compensation and tip/tilt correction as outlined in Section 6.D together with a tracking precision of $\sigma_t = 0.1''$.

The second main difference, however, is that the hit uncertainty $\sigma_r = \sqrt{(\sigma_p^2 + \sigma_t^2)}$ is not incorporated using the long-term beam radius as of Eq. (4) but by averaging the momentum obtained from Expedit over a large number of samples configured with random beam center offset from the target's center of mass following a normal probability distribution with a standard deviation of σ_r. Correspondingly, the expression for the (short-term) spot size reduces to $w(z) = M^2 \lambda\, z/(\pi\, w_0\, \sqrt{Str})$.

The resulting laser–debris interaction database was subsequently used in the transit simulations and interpolated there to derive the laser-imparted momentum for each elevation within the irradiation interval. Moreover, these data tables have been employed in the LTMT network simulations described below in Section 7.B.

The findings shown in Fig. 7 suggest the feasibility of laser-based collision avoidance for the majority of debris fragments and a significant number of payloads, rocket bodies, and mission-related objects up to a mass of a few hundred kilograms. For a particular mass, large deviations of Δv between different objects exist, which can be attributed to the great variety of area-to-mass ratios of the respective debris objects. Moreover, the comparison of the results with the analytical estimate assuming that the entire laser power reaches the debris object reveals the necessity to consider outshining losses, the need for compensation of turbulence-induced beam broadening, and the requirement of high-precision laser tracking and pointing.

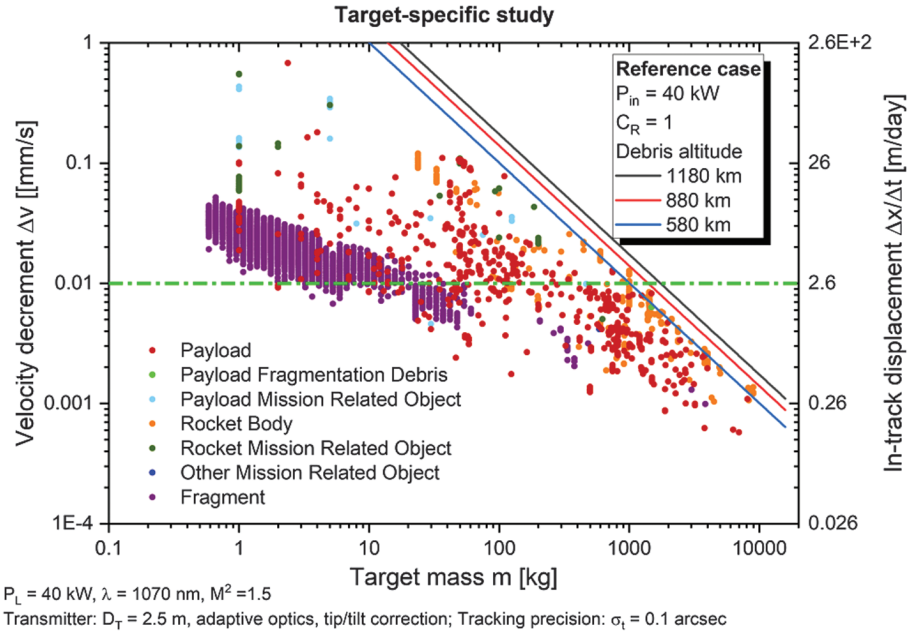

Fig. 7. Achievable velocity decrement for OOR debris targets in a direct MT station transit using a 40 kW high-power laser for momentum transfer, a 2.5 m diameter transmitter with adaptive optics and laser guide star, and tip/tilt correction for MT laser beam pointing and laser target tracking with a precision of 0.1 arcsecs. The randomness of target orientation and MT beam pointing offset has been considered in separate Monte Carlo simulations for each debris object.

7. COLLISION AVOIDANCE IN THE LOW EARTH ORBIT

A. Astrodynamics Constraints of Collision Avoidance

In a second feasibility study, laser-based MT has been analyzed with respect to astrodynamics constraints: For this purpose, conjunctions between the OOR objects have been simulated for a snapshot of the TLE catalog using Hoots's method for screening. The results were fed into Gaussian mixture clustering to identify characteristics such as orbital elements of target/chaser, typical conjunction angles, as well as the area-to-mass ratios of the involved objects. Based on these findings, parameters for the subsequent simulations have been selected. In addition, a hit probability model was implemented, considering laser beam pointing uncertainties together with orbit uncertainty. Based on this model, achievable MT success rates in terms of hit probability were derived, which also entered into the simulations to derive the astrodynamics constraints of laser momentum transfer. As additional crucial simulation parameters, the power in the bucket (PIB)—as a figure of merit for the laser power that actually arrives at the object—and the orbit prediction uncertainty have been considered.

To assess the feasibility of laser-based CA, i.e., yielding a collision probability $p_c < 10^{-4}$, two different network configurations have been analyzed. As lined out in greater detail in [6], it has been found that in the case of uncompensated atmospheric turbulence the required laser power is mostly much higher than what is currently technically feasible [except for a high MT success rate of 50%, a great time to event (6 days), and a high A/m ratio (0.008 m^2/kg), cf. Table 5]. The case of discarded atmospheric effects, however, may be a proxy for turbulence compensation by adaptive optics together with a large telescope aperture: here, the results in the first three rows promisingly demonstrate the feasibility of the concept for objects with a higher A/m but also, under fortunate conditions, for objects with smaller A/m.

B. Use Case #3: Networks for Laser Tracking and Momentum Transfer

In a more elaborate network optimization analysis using the simulation environment described in Section 4.B, it has been found that the collision rate can be reduced with LTMT by several orders of magnitude. As shown in greater detail in [5], two options have been analyzed here as a trade-off: i) using 24 LT stations but only as few sites with additional MT capability as possible and ii) using only LTMT sites. For the latter option, a network of 10 LTMT stations is sufficient to reduce the collision rate by more than 95% with respect to the case without MT (cf. Table 6). For the former option, however, already a single LTMT station is sufficient to meet this requirement if, in addition to that, 23 LT stations are used as well, i.e., the effort in momentum transfer to space debris is reduced here by an enhanced precision of orbital data from laser tracking, which can be understood as a trade-off between the efforts for LT precision and MT capability.

Table 6. Collision Rate for LTMT Networks in Comparison with Their Operation as Networks for Laser Tracking Only[a]

		Collision Rate	
Network	Size	w/o momentum transfer	with momentum transfer
SEN	5	$7.211 \cdot 10^{-6}$	$7.205 \cdot 10^{-6}$
LEN	8	$7.165 \cdot 10^{-6}$	$7.164 \cdot 10^{-6}$
LXN	9	$1.084 \cdot 10^{-34}$	$1.205 \cdot 10^{-35}$
LXN+	10	$2.029 \cdot 10^{-34}$	$9.448 \cdot 10^{-36}$
LXN++	11	$5.503 \cdot 10^{-34}$	$3.257 \cdot 10^{-36}$
XXN	24	$6.960 \cdot 10^{-38}$	$1.321 \cdot 10^{-91}$

[a]In the LTMT networks, all stations are equipped with a MT laser. LXN+ denotes the large extended network complemented by a single European station (San Fernando, SFEL, Spain), whereas for LXN++ a second European station (Matera, MATM, Italy) is included as well. In contrast to the simulations shown in Table 5, an action time frame of only 48 h has been considered here. A site-specific duty cycle has been employed, and simulations have been carried out for week A; cf. Table 1.

8. SUMMARY

Analyzing the astrodynamics constraints of laser tracking regarding in particular site-specific target visibility and orbit prediction uncertainty, the suitability of laser tracking for the generation of very accurate orbits, which can be used to commence laser momentum transfer, has been confirmed. Concerning laser tracking it can be stated that—in the use case of on-demand laser tracking as response to conjunction alerts—a global network of nine stations would be sufficient for the demanded reduction of both false alert rate and collision rate. However, for autonomous laser tracking, even 24 stations would be insufficient for continuous catalogue maintenance

Table 5. Required Laser Power for a Success Rate of 80% in Collision Avoidance with a Four-Station Network (Haleakala, Greenbelt, Borowiec, Mt. Stromlo), Data Taken from [6]

			Required Laser Power [kW]	
Turbulence	Duty Cycle	Action Time Frame [days]	A/m = 0.008 m^2/kg	A/m = 0.003 m^2/kg
Discarded	50%	6	8	22
Discarded	50%	4	19	51
Discarded	25%	6	21	55
Discarded	25%	4	47	126
Uncompensated	50%	6	52	140
Uncompensated	50%	4	125	334
Uncompensated	25%	6	135	359
Uncompensated	25%	4	318	849

for the given debris regime of more than 9000 selected objects (fragments, payloads, rocket bodies, mission-related objects, and so on).

For ground-based lasers, it can be stated that beam broadening together with beam wander due to atmospheric turbulence render collision avoidance by laser-based momentum transfer unfeasible if no measures for turbulence compensation are undertaken. Adaptive optics technology, however, provides a promising means to overcome this problem. It has been shown that using a transmitter of 2.5 m diameter, equipped with 300 actuators for the adaptive optics, operating with a bandwidth of 300 Hz, would yield successful CA for the majority of the objects in the OOR, provided a laser tracking uncertainty of only 0.1 arcsecs can be achieved. Moreover, a piezo-driven tip/tilt correction has to be applied, yielding a residual pointing uncertainty of approximately 0.01 arcsecs. This feasibility assessment is supported by a second feasibility study with respect to astrodynamics constraints, considering representative conjunction characteristics such as orbital elements, conjunction angles, and area-to-mass ratios of the involved objects. Laser beam pointing uncertainties have been reflected together with orbit uncertainty to assess the laser power that actually arrives at the object.

Regarding a station network for both laser tracking and momentum transfer, a network optimization study has been performed considering the optimum momentum transfer strategy for each configuration. It has been shown that operation of such a network can reduce the collision rate in the OOR by several orders of magnitude—either by using many (24) laser tracking stations of which only a single one exhibits capabilities for momentum transfer, or by using only 10 hybrid sites, which are for both tracking and momentum transfer.

9. OUTLOOK

Turbulence compensation is a crucial and promising technology regarding the feasibility of MT to space debris using high-power lasers. In general, outshining losses can be compensated for using a larger laser power, if available. Nevertheless, it should be considered that scaling of incident laser power, be it by adaptive optics usage or laser power scaling, does not only underlie technological constraints but also restrictions from operational safety: The absorbed heat $Q = \int_{t(\zeta_{\min})}^{t(\zeta_{\max})} (1 - R_A) P_{\text{in}}(t) \mathrm{d}t$ from the incident laser radiation cannot instantaneously be reradiated into space [32] but might lead to debris fragmentation by thermally induced stress or detonation of residual propellants or nondischarged batteries. Moreover, with an increased intensity the risk arising from possible specular backreflections is enhanced as well. Therefore, delicate studies on operational risks and their mitigation using an adequate normative and legal framework are recommended and appear worth the effort, since high-power lasers open up a unique possibility to perform agile on-demand CA for a multitude of debris objects.

For the implementation of a future LTMT network, it is proposed to start with the realization of the engineering station. Such a station, as conceptually shown in Fig. 8, would comprise laboratories for laser ranging, laser guide star, and momentum transfer laser systems, enabling both extensive testing and specification of single components and interfacing of units. All

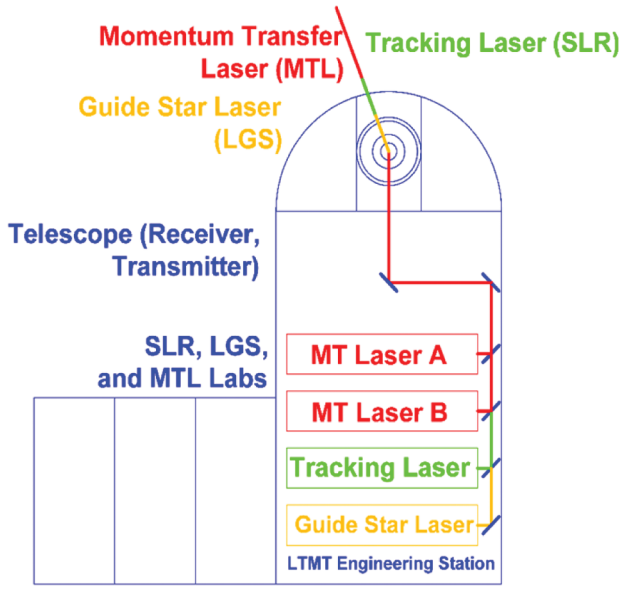

Fig. 8. Conceptual view of an LTMT engineering station comprising laboratories for testing and specification purposes.

network stations to be realized subsequently would be intended to operate autonomously. Hence, their realization depends on technology transfer of the testing and specification phases at the engineering station.

Under best-case assumptions, the whole network implementation might be feasible within a time span of only 5 years in which the technology transfer from the engineering station to the network stations would be undertaken after the first 2.5 years.

Admittedly, the debris situation in a LEO space environment is likely to undergo changes during those upcoming years of a possible network implementation, whereas our study deals with a snapshot of the OOR as of July 2019. The expected increase in space traffic, however, in particular related to megaconstellations, will lead to a significantly higher collision risk in space [33]. On top of that, SSA will presumably improve by newly implemented high-performance sensor systems [34], leading to a significant growth of the debris catalogue size, which, in turn, enlarges the resulting collision rate as well. Considering this, refinements will have to be undertaken continuously regarding not only the actual demand for collision avoidance but as well the real outcome of future LTMT networks when operational. Nevertheless, with a thoughtful prioritization of relevant conjunctions, the envisioned 10-station network of hybrid LTMT sites appears as a good starting point to tackle the challenge for space debris maneuvering for collision avoidance.

Funding. European Space Agency (4000127148/19/D/CT).

Acknowledgment. The data usage of DISCOS, Master-8, and CDM from ESA; TLE from USSTRATCOM; and weather data from ECMWF is thankfully acknowledged. Administrative support by Cristina Klaiber and Matthias Maurer as well as legal support by Anja Stojanov, Thierry Renard, and Elke Polch from DLR, and Caroline Thro from ESA for the execution of this study are greatly acknowledged.

Disclosures. The authors declare no conflicts of interest.

Data Availability. Debris data from the DISCOS database as well as debris population datasets from the Master-8 model are available from ESA upon reasonable request [35]. Conjunction data messages are not publicly available; however, TLE data can publicly be accessed [36]. Global weather data on cloud fraction from the ERA-Interim database [16] as well as data on aerosol optical depth from MACC-II [17] and CAMS Near-real time archive [18] are publicly available from the ECMWF. As a disclaimer it has to be noted that neither the European Commission nor ECMWF is responsible for any use of the downloaded weather data.

REFERENCES

1. H. Krag, S. J. Setty, A. Di Mira, I. Zayer, and T. Flohrer, "Ground-based laser for tracking and remediation – an architectural view," in *69th International Astronautical Congress (IAC)* (2018), paper IAC-18-A6.7.1.
2. S. Scharring, G. Wagner, J. Kästel, W. Riede, and J. Speiser, "Ablative collision avoidance for space debris in the Low Earth Orbit by a single multi-kJ pulse from a ground-based laser," presented at 22nd Advanced Maui Optical and Space Surveillance Technologies conference (AMOS)Maui, HI, September 14–17, 2021.
3. J. Mason, J. Stupl, W. Marshall, and C. Levit, "Orbital debris–debris collision avoidance," Adv. Space Res. **48**, 1643–1655 (2011).
4. F. Yang Yang, B. Nelson, J. Aziz, R. Carlino, A. Dono Perez, N. Faber, C. Foster, C. Frost, C. Henze, A. G. Karacalıoğlu, C. Levit, W. Marshall, J. Mason, C. O'Toole, J. Swenson, S. P. Worden, and J. Stupl, "LightForce photon-pressure collision avoidance: efficiency analysis in the current debris environment and long-term simulation perspective," Acta Astronaut. **126**, 411–423 (2016).
5. H. Dreyer, S. Scharring, J. Rodmann, W. Riede, C. Bamann, T. Flohrer, S. Setty, A. Di Mira, and E. Cordelli, "Future improvements in conjunction assessment and collision avoidance using a combined laser tracking/nudging network," in *8th European Conference on Space Debris (virtual)* (2021), paper 153.
6. C. Bamann, U. Hugentobler, S. Scharring, J. Kästel, and S. J. Setty, "Analysis of collision avoidance via ground-based laser momentum transfer," J. Space Saf. Eng. **7**, 312–317 (2020).
7. N. Hodgson and H. Weber, *Laser Resonators and Beam Propagation*, 2nd ed. (Springer, 2005).
8. R. L. Fante, "Electromagnetic beam propagation in turbulent media," Proc. IEEE **63**, 1669–1692 (1975).
9. R. K. Tyson, *Principles of Adaptive Optics*, 4th ed. (CRC Press, 2016).
10. D. A. Liedahl, A. Rubenchik, S. B. Libby, S. Nikolaev, and C. R. Phipps, "Pulsed laser interactions with space debris: target shape effects," Adv. Space Res. **52**, 895–915 (2013).
11. C. K. McInnes, *Solar Sailing: Technology, Dynamics, and Mission Applications* (Springer, 1999).
12. F. McLean, S. Lemmens, Q. Funke, and V. Braun, "DISCOS 3: an improved data model for ESA's database and information system characterizing objects in space," in *7th European Conference on Space Debris* (2017), paper 151.
13. H. Klinkrad and H. Sdunnus, "Concepts and applications of the MASTER space debris environment model," Adv. Space Res. **19**, 277–280 (1997).
14. J. J. Degnan, "Millimeter accuracy satellite laser ranging: a review," in *AGU Fall Meeting* (1993), pp. 133–162.
15. S. Scharring, J. Rodmann, and W. Riede, "Network performance analysis of laser-optical tracking for space situational awareness in the Lower Earth Orbit," in *20th Advanced Maui Optical and Space Surveillance Technologies conference (AMOS)* (2019), pp. 882–891.
16. European Center for Medium-Range Weather Forecast, "ERA-interim re-analysis," ECMWF, 2018, https://www.ecmwf.int/en/forecasts/dataset/ecmwf-reanalysis-interim.
17. European Center for Medium-Range Weather Forecast (ECMWF), "MACC-II reanalysis," ECMWF, 2018, https://www.ecmwf.int/en/forecasts/dataset/macc-reanalysis.
18. Copernicus Atmospheric Monitoring Service, "CAMS near-real-time archive," CAMS, 2018, https://apps.ecmwf.int/datasets/data/cams-nrealtime/.
19. R. A. McClatchey, R. W. Fenn, J. Selby, F. Volz, and J. Garing, *Optical Properties of the Atmosphere* (Air Force Cambridge Research Laboratories, 1972).
20. A. Tokovinin and T. Travouillon, "Model of optical turbulence profile at Cerro Pachón," Mon. Not. R. Astron. Soc. **365**, 1235–1242 (2006).
21. S. Scharring, L. Eisert, R.-A. Lorbeer, and H.-A. Eckel, "Momentum predictability and heat accumulation in laser-based space debris removal," Opt. Eng. **58**, 011004 (2018).
22. T. Hanada, J.-C. Liou, T. Nakajima, and E. Stansbery, "Outcome of recent satellite impact experiments," Adv. Space Res. **44**, 558–567 (2009).
23. M. K. Mulrooney, M. J. Matney, M. D. Hejduk, and E. S. Barker, "An investigation of global albedo values," in *9th Advanced Maui Optical and Space Surveillance Technologies Conference (AMOS)* (2008), pp. 615–624.
24. S. Marz, C. Bamann, and A. Schlicht, "ELT: multiple reflector identification and real-time time bias correction," in *ACES Workshop* (2018).
25. P. Lejba, T. Suchodolski, P. Michałek, J. Bartoszak, S. Schillak, and S. Zapasnik, "First laser measurements to space debris in Poland," Adv. Space Res. **61**, 2609–2616 (2018).
26. G. Kirchner, F. Koidl, F. Friederich, I. Buske, U. Volker, and W. Riede, "Laser measurements to space debris from Graz SLR station," Adv. Space Res. **51**, 21–24 (2013).
27. Z. Zhang, F. Yang, H. Zhang, Z. Wu, J. Chen, P. Li, and W. Meng, "The use of laser ranging to measure space debris," Res. Astron. Astrophys. **12**, 212–218 (2012).
28. Z. Zhongping, D. Huarong, T. Kai, W. Zhibo, and Z. Haifeng, "Development of laser measurement to space debris at Shanghai SLR station," in *7th European Conference on Space Debris* (2017), paper 255.
29. S. Scharring, J. Kästel, G. Wagner, W. Riede, E. Klein, C. Bamann, E. Döberl, D. Weinzinger, W. Promper, T. Flohrer, and A. Di Mira, "Potential of using ground-based high-power lasers to decelerate the evolution of space debris in LEO," in *8th European Conference on Space Debris (virtual)* (2021), paper 98.
30. C. Phipps, M. Birkan, W. Bohn, H.-A. Eckel, H. Horisawa, T. Lippert, M. Michaelis, Y. Rezunkov, A. Sasoh, W. Schall, S. Scharring, and J. Sinko, "Review: laser-ablation propulsion," J. Propul. Power **26**, 609–637 (2010).
31. G. A. Tyler, "Rapid evaluation of d0: the effective diameter of a laser-guide-star adaptive optics system," J. Opt. Soc. Am. A **11**, 325–338 (1994).
32. S. Scharring, R.-A. Lorbeer, and H.-A. Eckel, "Heat accumulation in laser-based removal of space debris," AIAA J. **56**, 2506–2508 (2018).
33. C. Parejo, N. Ortiz, and R. González, "Effect of mega constellations on collision risk in space," in *8th European Conference on Space Debris (virtual)* (2021), paper 246.
34. G. Fonder, M. Hughes, M. Dickson, M. Schoenfeld, and J. Gardner, "Space fence radar overview," in *International Applied Computational Electromagnetics Society Symposium (ACES)* (2019), pp. 1–2.
35. European Space Agency-European Space Operations Center (ESA/ESOC), "Space Debris User Portal," (DISCOS database, Master-8 model), ESA/ESOC, 2019, https://sdup.esoc.esa.int/.
36. United States Strategic Command (USSTRATCOM), "Two-line element orbital data," USSTRATCOM 2019, https://www.space-track.org/.